SOOT PARTICLE SIZE DISTRIBUTION MEASUREMENTS IN A TURBULENT ETHYLENE SWIRL FLAME

Gianluigi De Falco[a], Ingrid El Helou [b]*, Pedro M. de Oliveira[b], Mariano Sirignano [a], Ruoyang Yuan[c], Andrea D'Anna[a], Epaminondas Mastorakos[b]

[a] Dipartimento di Ingegneria Chimica, dei Materiali e della Produzione Industriale, Università degli Studi di Napoli "Federico II", P.le Tecchio 80, 80125, Napoli, Italy

[b] Department of Engineering, University of Cambridge, Cambridge CB2 1PZ, UK

[c] Department of Engineering, Loughborough University, Loughborough, LE11 3TU, UK

*** Corresponding Authors:** Ingrid El Helou (ie236@cam.ac.uk)

Colloquium: TURBULENT FLAMES

Supplemental Material Available

Words counting:

Main text:	4275
Equations:	0
Nomenclature:	0
References: 559	
Tables: 176	
Figure and Caption # 1: 185.5	
Figure and Caption # 2: 148	
Figure and Caption # 3: 129	
Figure and Caption # 4: 148	
Figure and Caption # 5: 165	
Figure and Caption # 6: 142	
Figure and Caption # 7: 295	
Figure and Caption # 8: 234.5	
Total:	**6227**

ABSTRACT

There is a need to better understand particle size distributions (PSDs) from turbulent flames from a theoretical, practical and even regulatory perspective. Experiments were conducted on a sooting turbulent non-premixed swirled ethylene flame with secondary (dilution) air injection to investigate exhaust and in-burner PSDs measured with a Scanning Mobility Particle Sizer (SMPS) and soot volume fractions (f_v) using extinction measurements. The focus was to understand the effect of systematically changing the amount and location of dilution air injection on the PSDs and f_v inside the burner and at the exhaust. The PSDs were also compared with planar Laser Induced Incandescence (LII) calibrated against the average f_v. LII provides some supplemental information on the relative soot amounts and spatial distribution among the various flow conditions that helps interpret the results. For the flame with no air dilution, f_v drops gradually along the centreline of the burner towards the exhaust and the PSD shows a shift from larger particles to smaller. However, with dilution air f_v reduces sharply where the dilution jets meet the burner axis. Downstream of the dilution jets f_v reduces gradually and the PSDs remain unchanged until the exhaust. At the exhaust, the flame with no air dilution shows significantly more particles with an f_v one to two orders of magnitude greater compared to the Cases with dilution. This dataset provides insights into soot spatial and particle size distributions within turbulent flames of relevance to gas turbine combustion with differing dilution parameters and the effect dilution has on the particle size. Additionally, this work measures f_v using both *ex situ* and *in situ* techniques, and highlights the difficulties associated with comparing results across the two. The results are useful for validating advanced models for turbulent combustion.

KEYWORDS: Soot, Turbulent non-premixed swirling flames, Particle size distributions, Scanning mobility particle sizer, Extinction.

1. INTRODUCTION

The Rich-Quench-Lean (RQL) concept, which uses swirling flows and cross-flow jets to form a relatively rich soot producing primary zone followed by a lean dilution zone promoting soot oxidation, has been a popular combustor technology for aero-engine applications [1]. In this configuration, the relative importance of the soot-forming and the soot-consuming regions depends on the respective residence times, turbulent mixing, mixture fraction distribution, and flow rate and location of the dilution jets, forming a large parameter space that needs to be studied systematically.

Most of the soot-focused research in turbulent non-premixed flames uses the canonical configuration of the axisymmetric jet [2, 3]. In this mainly uni-directional flow, there is a progressive mixing of the fuel, with the maximum mixture fraction shifting from very rich (unity close to the nozzle) to leaner than stoichiometric way downstream of the visible flame, hence allowing very insightful studies on soot formation and the development of reference test cases [2, 3]. However, in realistic combustors based on the RQL concept, the mixture fraction distribution is very much dependant on the flow patterns, swirl number, and strength and location of the dilution jets, which can affect both soot production and soot oxidation. Extensive work has been done with in-flame laser measurements on premixed and non-premixed turbulent swirling flames to investigate the effect of equivalence ratio, thermal power, pressure, turbulence and secondary air injection on soot formation [4-6]. These studies have shown the importance of understanding the time history of soot precursors and soot, and their dependence on local equivalence ratio, temperature, turbulence and mixing which lead to intermittency [4-10]. While some of these studies have looked at the effect of dilution in gaseous turbulent swirling flames [4-5, 9-10], less is known about the influence of varying the location of dilution air injection or the amount of dilution air introduced into the system. It should also be noted that the above studies on turbulent non-premixed swirl flames did not provide information on the particle size distribution (PSD) which is becoming of vital importance from a theoretical, practical and even regulatory perspective. Hence, further measurements of PSD in model RQL combustors are needed.

The many methods for analysing soot formation fall under either *ex situ* or *in situ* diagnostics. The former refers to particle sampling for improved structural and morphologic understanding of soot particles. Scanning mobility particle sizing (SMPS) is a powerful experimental technique widely applied to characterize the size distribution functions of aerosol particles. Coupled with dilution probe sampling, SMPS has been extensively used for measuring PSDs in combustion systems, since it provides rapid, direct and in-line measurements of PSDs in the range 1-100 nm [11-13]. This technique was applied to characterize sooting laminar premixed flames operated with different fuels [13-16] and sooting laminar diffusion flames [17]. More specifically, SMPS analysis revealed the bimodal nature of PSDs in sooting laminar flames and furnished relevant details for a deeper understanding of soot inception and growth mechanisms [18-21]. PSDs were also measured at the exhaust of practical combustion systems, generally confirming the presence of the bimodal shape [22].

In contrast, very few studies in the literature report applications of SMPS/probe sampling to turbulent flames. SMPS measurements have been reported in two papers with jet flames [23-24]. These studies reported PSDs along the centreline of C_2H_4/N_2 turbulent flames, in which the size distribution geometric mean was observed to increase monotonically with axial distance, finally exhibiting a mono-modal behaviour near the jet exit. The overall dilution ratio in the probing line was not measured, thus no absolute values of the PSDs were reported. Preliminary PSD measurements on the same RQL burner as this study have been reported in [25], and highlighted the change to the particle number only at the exhaust of the burner as the equivalence ratio was kept constant but the location of the dilution jets and air split was changed. For these reasons, this study builds on [25] while focusing on performing quantitative PSD measurements attained by a new probing system positioned both at the exhaust and inside of the burner. This study also sheds light on the smallest particles (down to 2 nm) formed not addressed in [25], while accurately avoiding undesired artefacts (coagulation phenomena) along the line.

The aim of the present work is to report PSD and f_v measurements in an ethylene non-premixed swirl burner, in order to promote our understanding of the effect of secondary air injection on soot

production and oxidation from RQL combustors, and to supplement previous work conducted on this burner using both probes and laser diagnostics [25, 26]. Probe measurements were performed both within and at the exit of the combustor, as both the amount and location of dilution air were systematically varied, to provide information on how the PSD and f_v changes with operating conditions and location in a flame configuration of practical relevance. Additionally, extinction experiments were conducted within the flame to quantify LII measurements reported previously [26]. Thus, this work aims to be a link between *in situ* and *ex situ* measurements, usually conducted separately, and discuss the difficulties when comparing the two. Finally, this work provides soot PSDs in swirl flames, which are a new contribution to the literature, and are expected to be useful for modern turbulent sooting flame models.

2. EXPERIMENTAL

The 11 kW burner is a turbulent, bluff body, swirl stabilized non-premixed ethylene/air burner operating at atmospheric pressure and identical to the one used in [25, 26]. Ethylene is axially injected along the axis through a straight tube 4 mm in diameter. Air at room temperature passes through a swirler consisting of 6 vanes and exits through an annular nozzle bounded by the bluff body internally (25 mm) and the nozzle diameter (37 mm). The burner operation is based on the RQL technology with four dilution jets positioned downstream of the burner inlet that can inject additional dilution air into the system. The burner has a square cross section (97x97 mm^2), is confined with four quartz plates (150 mm high), and has a contraction placed on top for the exhaust gases to exit. A schematic of the burner can be seen in Fig. 1, and Table 1 provides the experimental conditions. For all, the total fuel and air flow rates remain constant keeping the equivalence ratio constant at 0.3, but the air flow split between the primary annular ($U_{p,a}$) and the secondary dilution jets ($U_{d,a}$), and the location of these jets (H_j), is different. These parametric variations were chosen as the work of [25, 26] revealed that each change in air split, and dilution air location led to a varying degree of soot particle production both in

flame and at the exhaust stimulating further investigations in this paper. The Base Case is without any dilution air. Alicat mass flow controllers were used to control the flows with a measurement accuracy of ±0.8% (of the set value) and a full-scale accuracy of ±0.2%.

Table 1. Burner tested cases. Fuel velocity was kept constant at 15 m/s. $U_{d,a}$ is reported per jet. Air split is the ratio of primary to dilution air. Re is Reynold's number and is estimated based on $U_{p,a}$ alone.

Cases	$U_{p,a}$ (m/s)	$U_{d,a}$ (m/s)	Re	Air Split	H_j (mm)
Base	15.8	0	28430	100:0	0
1/3/5	12.7	40	22850	80:20	27/47/67
2/4/6	9.64	76	17350	60:40	27/47/67

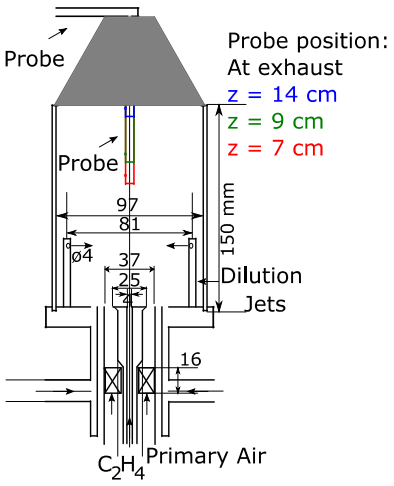

Figure 1. Schematic of the RQL burner with labels for the fuel, primary and dilution air inlets. The various locations of the sampling probe are depicted.

For the PSD measurements, combustion products were sampled from the flame using a tubular dilution probe. The use of probe sampling for measuring PSDs in combustion systems is widely adopted [11-14, 18]. However, in the present study a specific dilution probe, suitable to be placed both horizontally at the exhaust of the burner and vertically inside the burner, was designed and built with a pinhole size of 0.5 mm. A nitrogen flow rate of 10 l/min is used in a two-stage dilution sampling line to obtain an overall dilution ratio (DR) of 100, evaluated using a mass spectrometer. A calibration

procedure was performed to verify that DR is greater than the critical DR, i.e., the value above which particle coagulation in the line is suppressed, the shape of size distribution does not change, and the number eventually changes with inverse proportionality to the amount of dilution [11-13]. Details on the dilution probe and the sampling line can be found in the Supplemental Material.

Probe sampling was performed both at the exhaust of the burner and inside the burner with the locations marked in the schematic of Fig. 1. For sampling at the exhaust, the dilution probe was placed horizontally with respect to the surface of the burner, at the exit of the contraction after the combustion chamber. For sampling inside the chamber, the dilution probe was placed vertically along the burner axis and PSDs were measured at three different distances z between the probe pinhole and the burner surface, i.e., z=14 cm, z=9 cm and z=7 cm (see Fig. 1). These locations are downstream of where the dilution jets impinge, hence there is minimal disturbance on the flame.

The PSD measurements were performed using an SMPS system manufactured by TSI (SMPS Model 3936, see Supplemental Material for details) in the range 2.5-60 nm. The PSDs were all corrected for the dilution ratio and for diffusion losses of particles occurring in the dilution probe and in the sampling line, as already described in earlier works [18, 27].

Line of sight extinction measurements were performed to measure the soot volume fraction f_v and to calibrate previous Laser Induced Incandescence (LII) measurements performed for the Base Case and Cases 1 through 6 [26] since LII signals are proportional to f_v. A detailed explanation of the LII setup and experiments can be found in [26]. A continuous 1064 nm laser diode beam focused in the burner was used. A near-infrared wavelength was chosen to ensure minimal interference from soot precursors that absorb visible wavelengths. Additionally, this longer wavelength satisfies the Rayleigh scattering criterion ($\pi D/\lambda \ll 1$), ensuring that light scattered by the soot particles in the size range of interest (2.5-60 nm) is much lower than the light absorbed by them. The process followed for these measurements is widely used [2, 6, 28] and adheres to the Beer– Lambert–Bouguer's law. The transmitted to incident light ratios (I/I_o) were measured simultaneously using two photomultiplier tubes (Thorlabs DET36A) one placed before and the other after the burner, at a rate of 100 kHz and over

120 ms recorded using an oscilloscope. The largest source of measurement uncertainty derives from the complex function of the soot refractive index E(m) that may lead to errors up to a factor of 2 in f_v [6]. Here, an E(m, λ=1064nm) = 0.28 is chosen in accordance with [28]. Measurements were initially carried out in a laminar diffusion flame to calibrate the measurement system, and then on the RQL burner for the Base Case, and Cases 3 and 4. All the measurements were confined to the lower luminous part of the flame that is completely captured by the LII experiments. For further information on the calculations of extinction and quantitative LII refer to the supplemental information. Experiments were monitored and performed over short periods of time to ensure minimal temperature drift in the PMT response.

3. RESULTS AND DISCUSSION

3.1 Flame appearance

During burner operation changes to the flame shape and colour are visibly evident as dilution air is injected. The flame shortens as dilution air is introduced with 20% air flow through the jets, and the colour of the flame shifts from luminescent yellow to blue as dilution is increased to 40%. It is evident that, although the global equivalence ratio is the same in all the flames shown, the size and luminosity from the sooting region is different which motivates the study of soot number and particle size distributions both in-flame and at the exhaust. Photographs of the flame for the Base Case, and Cases 3 and 4 are available in the Supplemental Material for added context.

3.2 Particle size distributions

Figure 2 reports the number PSDs at the burner exhaust. The highest number concentration of particles is measured for particle diameters below 4 nm. With increasing particle size, the number concentration tends to decrease. However, a non-negligible amount of particles between 10 nm and 50 nm is measured, contributing significantly in terms of mass. On the other hand, the PSDs measured

for the six diluted cases are characterized by a similar but shifted trend to that of the Base Case with less particles produced.

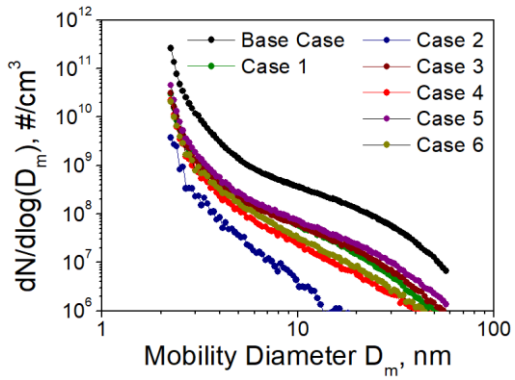

Figure 2. Number PSDs measured at the exhaust for Base Case and Cases 1 through 6.

The effect of introducing dilution air to the Base Case flame can be better appreciated by looking at Fig. 3, where the total particle number density N_{tot} and total particle volume fraction f_v^P from PSDs are shown. In Cases 1-3-5, the 80:20 split between the primary air and dilution air results in approximately one order of magnitude decrease in both N_{tot} and f_v^P with respect to the Base Case. On the other hand, the different dilution jet heights seems to have a minor impact on particle production, resulting only in a slight decrease of N_{tot} and f_v^P with decreasing jet heights from Case 5 (three bluff-body diameters height) to Case 1 (one bluff-body diameter height). In Cases 2-4-6 the 60:40 air split between the primary air and dilution air results in a further decrease of N_{tot} and f_v^P to two orders of magnitude lower than that of the Base Case for a jet height of one bluff-body diameter in Case 2. As the jets are moved further downstream at two and three bluff-body diameters, the reduction in N_{tot} and f_v^P is once again one order of magnitude lower than the Base Case. The effect of the dilution jets is expected to decrease with increasing height as they are positioned farther away from the bluff body. Previous work on this burner at these conditions has shown that the closer the jets are, and the higher the flow passing through them, the more they overlap with the central recirculation zone (CRZ), and thus have a greater influence on soot production and oxidation. This is further corroborated by the

results in Fig. 3 and is due to increased velocities, residence times, and improved mixing that reduce N_{tot} and f_v^P compared to the Base Case [26].

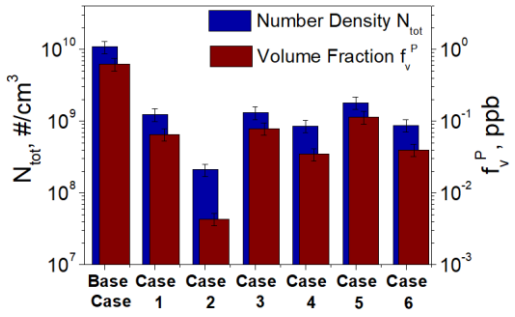

Figure 3. N_{tot} (right) and f_v^P (left) from PSDs for Base Case and Cases 1 through 6.

In contrast to the typical distributions measured by SMPS in laminar flames, the PSDs shown in Fig. 2 do not exhibit a clear bimodal shape, even if particles are detected over the whole size range. Such behaviour has been observed in the only other experimental PSD study of turbulent flames published so far [23, 24], as well as in computational works [29, 30]. These authors suggested that, for any sampling location, the measured particle distribution is the average of an ensemble of several instantaneous distributions, any of which differs from the others since soot particles follow different path lines due to the turbulent nature of the flow, resulting in the loss of a possible bimodality [23, 24, 29, 30].

The number PSDs measured for the Base Case at three different locations inside the burner are shown in Fig. 4, together with the PSD measured at the exhaust. Within the experimental uncertainties, the PSD at z=7 cm shows a significant change in shape compared to the exhaust PSDs of Fig. 2 and the other PSDs of Fig. 4, given by a reduction of particle number below 10 nm and a significant increase in the amount of particles produced between 10 nm and 50 nm. This results in a slight increase in the total number concentration from N_{tot}=7.0 ±1.5 x 10^9 #/cm^3 at z=7 cm to N_{tot}=1.0 ±0.2 x 10^{10} #/cm^3 at the exhaust, and a decrease in the total volume fraction from f_v^P=6.5 ±1.0 ppb at z=7 cm to f_v^P=0.8 ±0.18 ppb at the exhaust. On the other hand, PSDs at z=9 cm and z=14 cm are identical and

overlap with the PSD measured at the exhaust of the burner. This suggests that as particles are formed and move towards the exhaust they are oxidized and the PSD shifts from large particles inside the burner to small particles downstream of the flame and at the exhaust.

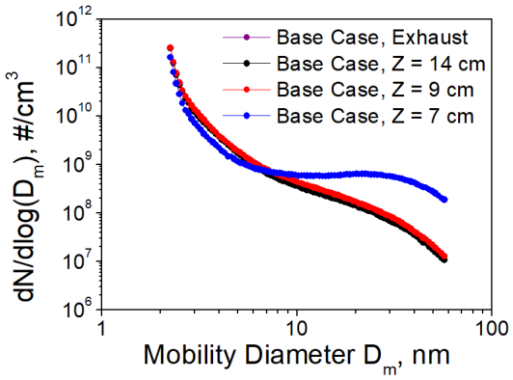

Figure 4. Number PSDs measured at the exhaust and at three z for the Base Case.

Cases 3 and 4 revealed an order of magnitude drop in f_v^p in Fig. 3 at the exhaust, as well as a visible change in flame shape in Fig. S1 of the supplemental material compared to the Base Case, and were therefore chosen for further PSD measurements inside the burner as shown in Fig. 5. For both Cases, the PSDs measured at the exhaust and at any location inside the burner do not present any significant differences in terms of shape and intensity, resulting in the same values of N_{tot} and f_v^P within the experimental uncertainties. This result is expected as the dilution jets are placed at a height of 47 mm, and the injection of dilution air reduces the size of the flame and restricts the fuel jet penetration and the propagation of soot particles downstream of the injection point. Therefore, at the probe positions between z=7 cm to the exhaust, the dilution jets have already oxidized the formed soot leading to negligible changes in the PSDs.

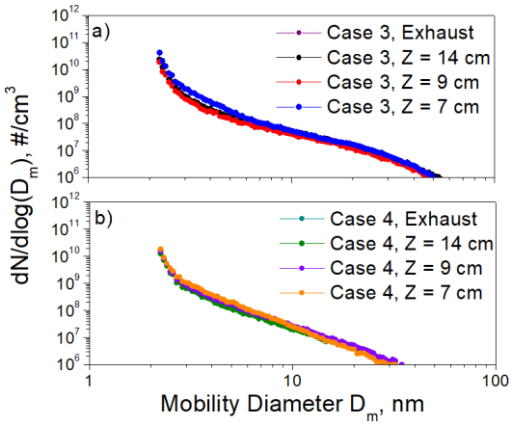

Figure 5. Number PSDs measured at the exhaust and at three z for Case 3 (a) and Case 4 (b).

3.3 Extinction Measurements

In addition to the DMA measurements, in-flame extinction measurements were performed to investigate the change in integrated soot volume fraction (f_v^e) along the centreline of the burner for the Base Case and Cases 3 and 4 (Fig. 6). Cases 3 and 4 were chosen because of their lower detected LII signal compared to the Base Case as is seen in Fig. 7. The Base Case experiences a gradual drop in f_v^e with height from 105 ppb.m to 65 ppb.m towards the exhaust. A sharper drop in f_v^e past 1.5 cm is observed, from 105 ppb.m to 76 ppb.m and 68 ppb.m for Cases 3 and 4 respectively, as the dilution jets are approached. Past the dilution jets and their oxidation, the drop in f_v^e is once again gradual as the f_v^e approaching the exhaust for Cases 3 and 4 is 64 ppb.m and 57 ppb.m respectively. The last two extinction measurements were performed at heights identical to the probe measurements at a z=7 cm and 9 cm. It should be noted that the upper cut-off limit for the DMA measurements is 60 nm, while the extinction measures a wider range of particles. Additionally, the extinction measurements are integrated over the beam path, while probe measurements are local; quantitative comparisons might be misleading without taking these differences into account. The extinction experiments show that the integrated f_v^e drops by 35% in the Base Case as the exhaust is approached, while it drops by 45% for Case 4. Considering the length of the flame (the luminous regions of Fig. S1 in the supplemental material), it wouldn't be expected that f_v^p from centerline PSDs would agree with measurements of

integrated f_v^e while taking into account the uncertainties in both experiments, especially since soot presence peaks within the CRZ (which would contribute greatly to the integrated f_v^e measured) and not along the burner centreline as will be shown next.

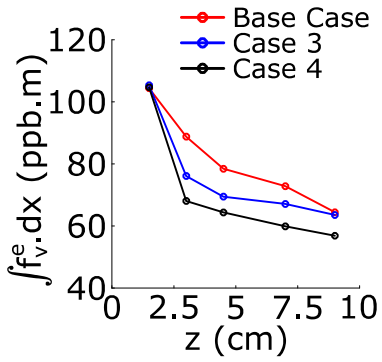

Figure 6. Integrated soot volume fraction from line-of-sight extinction across several heights along the centreline of the flame.

Time-averaged soot volume fraction from LII (f_v^l) is shown in Fig. 7 for the Base Case and Cases 3 and 4. The integrated f_v^e at a height of 1.5 cm in Fig. 6 reveals that all three Cases produce the same f_v^e at this height. However, the integrated LII signal at this height for all three Cases varies in magnitude. This is attributed to: the LII setup's tuning towards larger soot particles [26], the extinction setup's wider particle size range, and finally, with the dilution jets there is oxidation that reduces the size of larger particles to values outside the range captured by LII. Still, knowing that the Base Case is the most sooting case, with the highest LII signal as well as f_v^e and f_v^p, an estimation of f_v^l from LII was thus based on the Base Case values and applied to all other Cases. These results reveal a f_v^l in the range of 0 – 0.52 ppb for the Base Case and Case 3, and two orders of magnitude lower in Case 4. The LII experiments do reveal a gradual drop in f_v^l in the Base Case compared to a sharp drop in Cases 3 and 4 along the burner height similarly to Fig. 6. Comparing to Fig. 4 and Fig. 5, the LII signal is unable to capture the total amount of soot present within the burner with a factor of 10 difference between the f_v^l and the PSD results. In the Base Case, soot particles oxidize as they propagate

downstream leading to a lower LII signal and a discrepancy with the PSD measurements as only the larger soot particles are captured using LII. The dilution introduced in Cases 3 and 4 reduces soot formation and increases soot oxidation further contributing to the discrepancy of having no detected LII signal beyond z= 3 cm, but having measured f_v^p in the range of 0.03 - 0.09 ppb from z= 7 cm to the exhaust. Thus, the lower f_v^l caused by the LII bias, the lower DMA size range, the LII field of view, and the measurement location must always be taken into account when comparing across techniques. These results highlight the importance of a combination of experiments, as the extinction and PSD measurements reveal that there is in fact more soot particles, albeit smaller ones compared to the Base Case, formed in Cases 3 and 4.

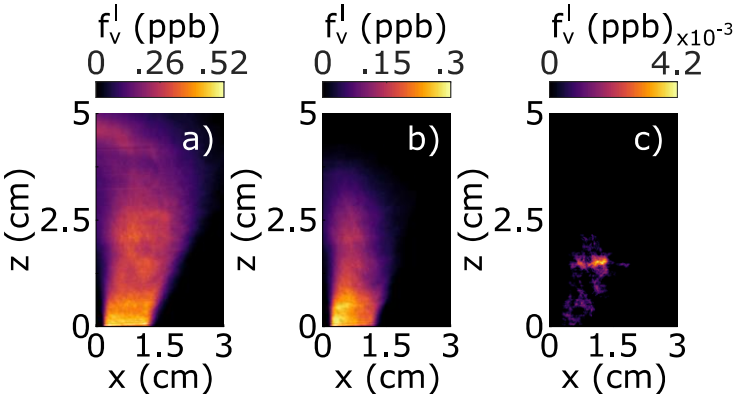

Figure 7. Time averaged f_v^l showing one half of the flame front for the Base Case (a), Case 3 (b) and Case 4 (c).

Finally, radial distributions of f_v^l are shown at various heights of the flame in Fig. 8. These distributions reveal that the highest concentration of soot forms close to the bluff body at z= 0.5 cm and peaks within the CRZ. The same f_v^l distribution is evident at all z for the Base Case with the f_v^l peaking in the CRZ. The distribution for Case 3 maintains the same shape but drops in magnitude as the dilution jets are approached, leading to a negligible amount of f_v^l detected past the jets. Finally, for Case 4, there is a very low amount of f_v^l detected at all z past 0.5 cm, and what is detected is equivalent to less than 2% that of the Base Case at 0.5 cm. The combination of optical diagnostics and sampling

experiments reveal that there is a significant reduction in total $f_v^{p,e,l}$ and N as dilution is introduced, which inhibits particle formation and oxidizes larger particles.

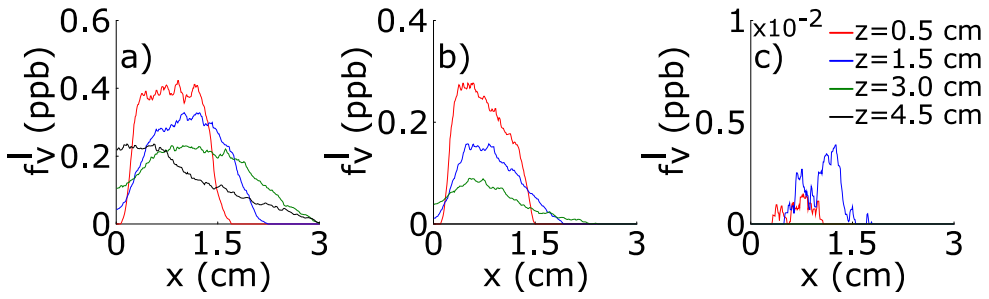

Figure 8. Radial distributions of f_v^l for half the flame at several heights for the Base Case (a), Case 3 (b) and Case 4 (c).

4. CONCLUSIONS

A detailed study of soot volume and particle size distributions both in-flame and at the exhaust for a turbulent non-premixed swirling flame revealed insights into the sooting tendencies of this flame when dilution air is added at different heights along the burner and at different ratios. Results of the PSDs at the exhaust revealed that the dilution jets reduce f_v^P by one to two orders of magnitude compared to the Base Case, and the closer the jets are to the base of the burner the lower is the f_v^P at the exhaust. PSDs measured within the burner show that f_v^P decreases by a factor of 10 for the Base Case as the exhaust is approached; while the PSDs of the Cases with dilution air are identical both in the burner and at the exhaust. This suggests that dilution air promotes effective soot oxidation within the burner. Integrated f_v^e along the height of the burner at the centreline show that while all the Cases produce the same f_v^e close to the bluff body, the behaviour downstream changes as the jets are approached. While the Base Case f_v^e reduces gradually with height, for the dilution Cases there is a sharp drop in f_v^e as the dilution jets are approached, followed by a gradual drop farther downstream from the jets. LII images, which may miss the smaller particles, reveal that soot forms off-axis and upstream of the dilution jets, and that there is virtually no LII signal in the highly diluted flame, although there are many small

particles sampled by the probe and the light extinction. The presence of large number of small particles at the burner exit, even in flames that are not very visibly sooty, will drive further research on this topic. Future work will be devoted to tuning the LII experiments to capture a wider range of soot particles within the burner. LII signals can be detected slightly upstream of the probe locations, where the flame terminates, in order to improve comparisons across measurement techniques while taking into account the different range limitations of each.

ACKNOWLEDGEMENTS

The authors would like to thank S. Gabra at Chem. Eng. Cambridge for the MS analysis. We would also like to thank the European Commission Clean Sky 2 project Leafinnox (project number 831804), Rolls Royce, and the EPSRC CTD in Gas Turbine Aerodynamics.

REFERENCES

[1] S. Samuelsen, Rich Burn, Quick-Mix, Learn Burn (RQL) Combustor, Gas Turbine Handbook, U.S. Department of Energy, 2006 p. 227.

[2] N. H. Qamar, Z. T. Alwahabi, Q. N. Chan, G. J. Nathan, D. Roekaerts, K. D. King, Soot volume fraction in a piloted turbulent jet non-premixed flame of natural gas, Combust. Flame 156 (7) (2009) 1339–1347.

[3] S. M. Mahmoud, G. J. Nathan, Z. T. Alwahabi, Z. W. Sun, P. R. Medwell, B. B. Dally, The effect of exit strain rate on soot volume fraction in turbulent non-premixed jet flames, Proc. Combust. Inst. 36 (2017) 889–897.

[4] K. P. Geigle, W. Meier, R. Hadef, Soot formation and flame characterization of an aero-engine model combustor burning ethylene at elevated pressure, J. Eng. Gas Turbines Power. 136 (2014) 021505.

[5] K. P. Geigle, R. Hadef, M. Stöhr, W. Meier, Flow field characterization of pressurized sooting swirl flames and relation to soot distributions, Proc. Combust. Inst. 36 (2017) 3917–3924.

[6] M. Roussillo, P. Scouflaire, S. Candel, and B. Franzelli, Experimental investigation of soot production in a confined swirled flame operating under perfectly premixed rich conditions, Proc. Combust. Inst. 37 (2018) 893-901.

[7] L. Wang, S. Chatterjee, Q. An, A. M. Steinberg, Ö. L. Gülder, Soot formation and flame structure in swirl-stabilized turbulent non-premixed methane combustion, Combust. Flame 209 (2019) 303–312.

[8] L. Y. Wang, C. K. Bauer, Ö. L. Gülder, Soot and flow field in turbulent swirl-stabilized spray flames of Jet A-1 in a model combustor, Proc. Combust. Inst. 37 (2019) 5437–5444.

[9] K. P. Geigle, J. Zerbs, M. Köhler, M. Stöhr, W. Meier, Experimental Analysis of Soot Formation and Oxidation in a Gas Turbine Model Combustor Using Laser Diagnostics, J. Eng. Gas Turbines Power 133 (2011) 121503-1-121503-8.

[10] K. P. Geigle, M. Köhler, W. O'Loughlin, W. Meier, Investigation of soot formation in pressurized swirl flames by laser measurements of temperature, flame structures and soot concentrations, Proc. Combust. Inst. 35 (2015) 3373–3380.

[11] M.M. Maricq, S.J Harris, J.J Szente, Soot size distributions in rich premixed ethylene flames, Combust. Flame 132 (2003) 328–342.

[12] B. Zhao, Z. Yang, J. Wang, M.V. Johnston, H. Wang, Analysis of soot nanoparticles in a laminar premixed ethylene flame by scanning mobility particle sizer, Aerosol Sci. Technol. 37 (2003) 611-620.

[13] L.A. Sgro, A. D'Anna, P. Minutolo, Charge fraction distribution of nucleation mode particles: New insight on the particle formation mechanism, Combust. Flame 158 (2011) 1418–1425.

[14] A.D. Abid, E.D. Tolmachoff, D.J. Phares, H. Wang, Y. Liu, A. Laskin, Size distribution and morphology of nascent soot in premixed ethylene flames with and without benzene doping, Proc. Combust. Inst. 32 (2009) 681–688.

[15] J. Camacho, S. Lieb, H. Wang, Evolution of size distribution of nascent soot in *n*- and *i*-butanol flames, Proc. Combust. Inst. 34 (2013) 1853–1860.

[16] M. Conturso, M. Sirignano, A. D'Anna, Effect of 2,5-dimethylfuran doping on particle size distributions measured in premixed ethylene/air flames, Proc. Combust. Inst. 36 (2017) 985-992.

[17] M. Kazemimanesh, A. Moallemi, J.S. Olfert, L.W. Kostiuk, Probe sampling to map and characterize nanoparticles along the axis of a laminar methane jet diffusion flame, Proc. Combust. Inst. 36 (2017) 881–888.

[18] M. Commodo, G. De Falco, A. Bruno, C. Borriello, P. Minutolo, A. D'Anna, Physicochemical evolution of nascent soot particles in a laminar premixed flame: From nucleation to early growth, Combust. Flame 162 (2015) 3854-3863.

[19] M. Commodo, G. Tessitore, G. De Falco, A. Bruno, P. Minutolo, A. D'Anna, Further details on particle inception and growth in premixed flames, Proc. Combust. Inst. 35 (2015) 1795-1802.

[20] M. Sirignano, A. D'Anna, Coagulation of combustion generated nanoparticles in low and intermediate temperature regimes: An experimental study, Proc. Combust. Inst. 34 (2013) 1877-1884.

[21] F. Carbone, M. Attoui, A. Gomez, Challenges of measuring nascent soot in flames as evidenced by high-resolution differential mobility analysis, Aerosol Sci. Technol. 50 (2016), 740-757.

[22] S. J. Harris, M.Matti Maricq, Signature size distributions for diesel and gasoline engine exhaust particulate matter, J. Aerosol Sci. 32 (2001)749-764.

[23] W. Boyette, S. Chowdhury, W. Roberts, Soot Particle Size Distribution Functions in a Turbulent Non-Premixed Ethylene-Nitrogen Flame, Flow Turbulence Combust. 98 (2017) 1173–1186.

[24] S. Chowdhury, W. Boyette, W. Roberts, Time-averaged probability density functions of soot nanoparticles along the centerline of a piloted turbulent diffusion flame using a scanning mobility particle sizer, J. Aerosol Sci. 106 (2017) 56–67.

[25] T. Tracy, J. A. M. Sidey, E. Mastorakos, A lab-scale Rich-Quench-Lean (RQL) combustor for stability and soot investigations. AIAA aerospace science meeting (2018).

[26] I. El Helou, A. W. Skiba, E. Mastorakos, Investigation of soot production and oxidation in a lab-scale Rich-Quench-Lean (RQL) burner using in situ laser diagnostics, Flow Turbulence Combust. (2020).

[27] P. Minutolo, A. D'Anna, A. D'Alessio, On detection of nanoparticles below the sooting threshold, Combust. Flame 152 (2008) 287-292.

[28] M. Köhler, K. P. Geigle, W. Meier, B. M. Crosland, K. A. Thomson, G. J. Smallwood, Sooting turbulent jet flame: characterization and quantitative soot measurements, Appl. Phys. B Lasers Opt. 104 (2011) 409–425.

[29] K. Netzell, H. Lehtiniemi, F. Mauss, Calculating the soot particle size distribution function in turbulent diffusion flames using a sectional method, Proc. Combust. Inst. 31 (2007) 667–674.

[30] M. Lucchesi, A. Abdelgadir, A. Attili, F. Bisetti, Simulation and analysis of the soot particle size distribution in a turbulent nonpremixed flame, Combust. Flame 178 (2017) 35-45.

FIGURE CAPTIONS

Figure 1. Schematic of the RQL burner with labels for the fuel, primary and dilution air inlets. The various locations of the sampling probe are depicted.

Figure 2. Number PSDs measured at the exhaust for Base Case and Cases 1 through 6.

Figure 3. N_{tot} (right) and f_v^P (left) from PSDs for Base Case and Cases 1 through 6.

Figure 4. Number PSDs measured at the exhaust and at three z for the Base Case.

Figure 5. Number PSDs measured at the exhaust and at three z for Case 3 (a) and Case 4 (b).

Figure 6. Integrated soot volume fraction from line-of-sight extinction across several heights along the centreline of the flame.

Figure 7. Time averaged f_v^l showing one half of the flame front for the Base Case (a), Case 3 (b) and Case 4 (c).

Figure 8. Radial distributions of f_v^l for half the flame at several heights for the Base Case (a), Case 3 (b) and Case 4 (c)x